Chemistry–A European Journal
Research Article
doi.org/10.1002/chem.202200712
Chemistry Europe
European Chemical Societies Publishing
www.chemeurj.org

Structural Phase Transitions and Magnetic Superexchange in $M^{I}Ag^{II}F_3$ Perovskites at High Pressure**

Łukasz Wolański,[a] Marvin Metzelaars,[b] Jan van Leusen,[b] Paul Kögerler,*[b, c] and Wojciech Grochala*[a]

This work commemorates the 200th anniversary of the birth of Louis Pasteur and the 100th anniversary of the birth of Rudolf Hoppe.

Abstract: Pressure-induced phase transitions of $M^{I}Ag^{II}F_3$ perovskites (M = K, Rb, Cs) have been predicted theoretically for the first time for pressures up to 100 GPa. The sequence of phase transitions for M = K and Rb consists of a transition from orthorhombic to monoclinic and back to orthorhombic, associated with progressive bending of infinite chains of corner-sharing $[AgF_6]^{4-}$ octahedra and their mutual approach through secondary Ag···F contacts. In stark contrast, only a single phase transition (tetragonal→triclinic) is predicted for $CsAgF_3$; this is associated with substantial deformation of the Jahn–Teller-distorted first coordination sphere of Ag^{II} and association of the infinite $[AgF_6]^{4-}$ chains into a polymeric sublattice. The phase transitions markedly decrease the coupling strength of intra-chain antiferromagnetic superexchange in $MAgF_3$ hosts lattices.

Introduction

There has been a great upsurge of interest in halide perovskites, particularly due to their ability to serve as photochemically active materials in solar cells.[1,2] Among all halides, fluorides tend to be the least studied, as they usually exhibit very large fundamental band gaps, and the corresponding perovskites are poor electric conductors. Divalent silver (Ag^{2+}) fluorides stand out in this group due to their moderate band gaps approaching the UV/vis edge,[3] and substantial involvement of F(2p) orbitals in covalent chemical bonding to Ag.[4–6] These features also permit the markedly strong superexchange between spin-$^1/_2$ $4d^9$ metal centers mediated by fluoride bridges.[7,8] The structures and selected properties of $MAgF_3$ perovskites (M = K, Rb, Cs), have been studied by Hoppe et al. half a century ago,[9] and they have been critically scrutinized more recently by one of our groups.[10–13] It turns out that dark brown $MAgF_3$ perovskites (M = K, Rb, Cs) may serve as hosts of exceptionally strong antiferromagnetic superexchange characterized by superexchange constants J_{1D} ranging from about −100 meV (ca. −800 cm^{-1}) for K^+ to −180 meV (ca. −1450 cm^{-1}) for the Cs^+ analogue.[8,11] While the ambient-pressure crystal structures of the $MAgF_3$ series (M = K, Rb, Cs) are known, their polymorphism is a virtually uncharted area, in contrast to the pressure-induced phase transitions for their parent compound, AgF_2.[14,15]

Therefore, we here have explored theoretically the impact of high pressures (up to 100 GPa) on the crystal structures as well as on the magnetic properties of the $MAgF_3$ series. By comparing results obtained for M = K, Rb and Cs, we aim at understanding the trends governing their structural preferences and magnetic characteristics.

Results and Discussion

Our approach is based on solid-state density functional theory (DFT) computations carried out with the help of self-learning algorithms (XtalOpt r11.0)[16,17] (see the Computational Details), while accounting for ferromagnetic and diverse antiferromagnetic models (see the Supporting Information).

Calculations carried out for $p = 0$ GPa and $T = 0$ K result in delivered ground-state structures in agreement with experiment[9–11] and with a recent computational study.[12,13] Both the K and Rb salts crystallize in orthorhombic *Pnma* cells (Figure 1; distorted $GdFeO_3$-type perovskite) while the Cs analogue adopts a higher symmetry tetragonal *I*4/*mcm* cell (also representing a distorted perovskite). The infinite AgF_3^- chains are bent for the K salt, and are ideally linear for the Cs

[a] Dr. Ł. Wolański, Prof. W. Grochala
Centre of New Technologies, University of Warsaw,
S. Banacha 2c, 02-097 Warsaw (Poland)
E-mail: w.grochala@cent.uw.edu.pl
[b] Dr. M. Metzelaars, Dr. J. van Leusen, Prof. P. Kögerler
Institute of Inorganic Chemistry
RWTH Aachen University
52074 Aachen (Germany)
E-mail: paul.koegerler@ac.rwth-aachen.de
[c] Prof. P. Kögerler
Peter Grünberg Institute (PGI-6)
Forschungszentrum Jülich GmbH
52425 Jülich (Germany)

[**] *A previous version of this manuscript has been deposited on a preprint server (https://doi.org/10.48550/arXiv.2203.02312).*

Supporting information for this article is available on the WWW under https://doi.org/10.1002/chem.202200712

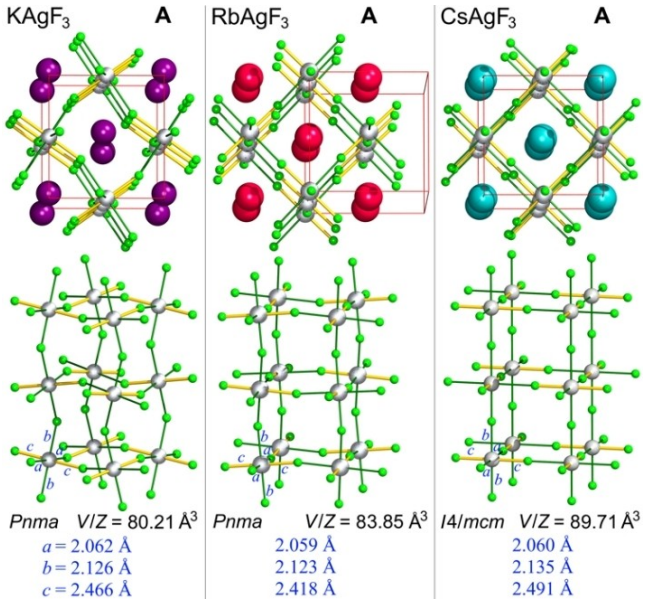

Figure 1. Minimum-enthalpy equilibrium structures of the **A** isomers of $MAgF_3$ (M = K, Rb and Cs). Only Ag–F bonds are shown for clarity, and M^+ cations are omitted in the bottom figures. Unit cell edges are emphasized as red lines. Lengths of Ag–F bonds (*a*, *b*, *c*) are indicated by different colors (green: shorter, yellow: longer).

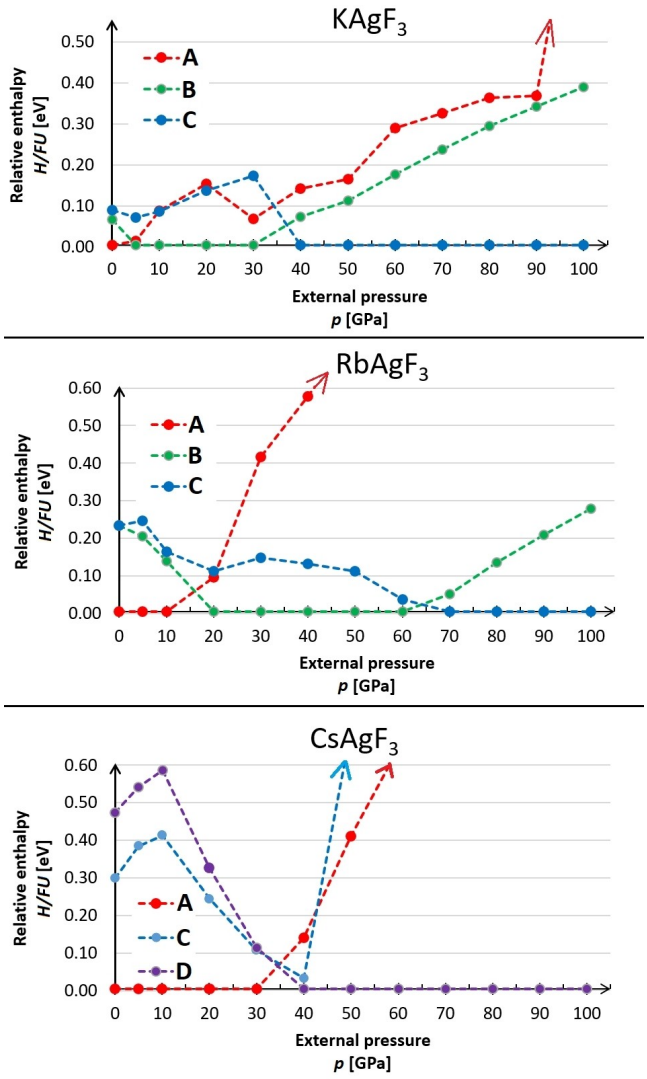

Figure 2. Influence of external pressure on minimum-enthalpy equilibrium structures of $MAgF_3$. For each member of the series, the relative enthalpies per formula unit, *H*/FU, of the relevant polymorphs are shown. The enthalpy of the most stable form for each external pressure defines the energy origin.

salt. The Rb structure represents an intermediate between these two structures. The AgF_3^- chains are characterized by strong antiferromagnetic superexchange, and thus the ranking of J_{1D} values follows closely the Ag–F–Ag angle. Due to marked similarity of the *Pnma* and *I*4/*mcm* cells these polymorphs are labeled here jointly as structure **A** (Figure 1).

Our calculations reveal the presence of two consecutive phase transitions for $KAgF_3$ and $RbAgF_3$ but only one for $CsAgF_3$ (Figure 2). Importantly, the polymorphs of K and Rb derivatives are identical; we denote them here as **B** and **C**, and their crystal structures are shown in Figure 3. On the other hand, an entirely different form labeled **D** is the sole high-pressure polymorph of $CsAgF_3$ up to 100 GPa (Figures 2 and 3). As it could be expected, the pressure needed for the first phase transition to occur varies from around 4.5 GPa for K, via about 12.5 GPa for Rb up to approximately 35 GPa for Cs analogue (Figure 2). On the other hand, the next phase transition for K salt is expected at 38 GPa, for Rb one at 64 GPa, while it is absent for Cs up to 100 GPa. Such behavior shows a clear and monotonic trend in the series of alkali metal cations with strongly increasing ionic radius.

B is monoclinic, $P2_1/m$, whereas **C** is orthorhombic and it formally belongs to the same space group as the ground state structure **A** (*Pnma*) for K and Rb derivatives. Yet, there are noticeable differences between them (Figure 3). For example, computation for form **A** of $KAgF_3$ at 10 GPa reveals the following coordination sphere of Ag: 2×2.09 Å (for Ag–F bonds parallel to the propagation direction of the infinite chains), and 2×2.03 Å plus 2×2.30 Å (yielding an anti-ferrodistortive bond pattern within $[AgF_2]$ sheets). Simultaneously, form **B** of this compound at 10 GPa features the following Ag–F bonds: 2×2.08 Å (for Ag–F bonds parallel to the propagation direction of the infinite chains), and 2×2.04 Å plus 2×2.40 Å (within $[AgF_2]$ sheets). Clearly, the longest Ag–F distance in the first coordination sphere of Ag is less squeezed in **B** than in **A**, resulting in more favorable enthalpy for the former at 10 GPa.

In this way, the Jahn–Teller distortion of the AgF_6 octahedron may be more pronounced,[18,19] and this is associated with a smaller local strain than for the structure **A**. There are also differences in the first coordination sphere of the alkali atoms in each forms. For example, in the case of $KAgF_3$ at 10 GPa, K^+ is surrounded by nine fluoride ligands in structure **A** (at 2.51, 2×2.52, 2.61, 2×2.69, 2×2.72, and 2.85 Å) with an average bond length of 2.65 Å. Simultaneously, in the polytype **B** the coordination sphere of K consists of eight bonds: 2.53, 2×2.53, 2.58, 2.60, 2×2.62, and 2.97 Å, with an average bond length of 2.62 Å. Thus, the expected increase of the coordination number

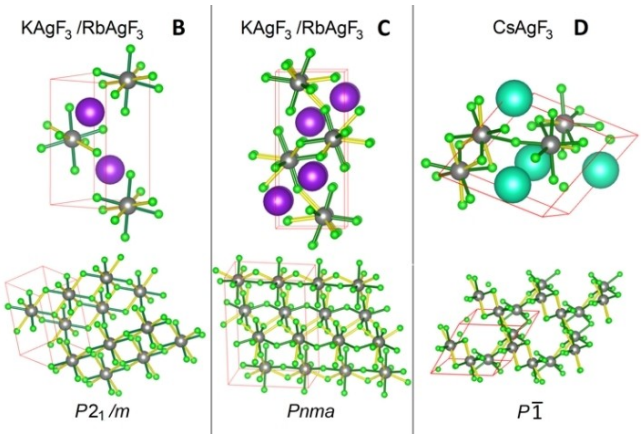

Figure 3. Minimum-enthalpy equilibrium structures of the **B** polymorphs of $KAgF_3$/$RbAgF_3$ under external pressure of 30 GPa (left), **C** polymorphs of $KAgF_3$/$RbAgF_3$ (middle) and the **D** form of $CsAgF_3$ at 100 GPa (right). The Ag–F bonds are shown in green (short bonds) and yellow (longer bonds). In some cases, M^+ cations are omitted for clarity. Unit cells have been emphasized by solid lines.

of alkali metal at elevated pressure[20] is not observed and as such cannot drive the **A**→**B** structural transition.

Similar conclusions related to local Jahn–Teller effect and to coordination sphere of alkali metal cation may be reached for the respective **A**→**B** phase transition for the $RbAgF_3$ homologue. The AgF_6 octahedron at 20 GPa exhibits the following bond lengths: 2×2.01, 2×2.02, and 2×2.21 Å in structure **A**, and 2×2.02, 2×2.09, and 2×2.56 Å in structure **B**. Simultaneously, the coordination number of Rb drops from 11 in **A** to 10 in **B**. Again, this is not the change of the coordination sphere of alkali metal cation, but rather the structural flexibility of structure **B** in releasing the strain associated with squeezing of the AgF_6 octahedra, which is beyond the **A**→**B** phase transition.

And what are the structural changes associated with the second structural phase transition, **B**→**C**? Inspection of the crystal structure of $KAgF_3$ at 40 GPa in structure **B** and **C** leads to the following conclusions: the bonding pattern in the first coordination sphere of Ag changes from a more regular one resembling 4+4 coordination, 2×2.00, 2×2.06 plus 2×2.43 and 2×2.44 Å, to a highly irregular one 2.00, 2.05, 2.09, 2.11, 2.28, plus 2.44 and 2.46 Å, resembling (4+1)+2 coordination. In other words, AgF_4 squares with four secondary contacts are substituted by irregular AgF_5 pyramids with two additional longer interactions. A similar mechanism has been seen to drive the pressure-induced phase transitions in binary AgF_2, where quasi-pentacoordinated units were detected.[14,15]

The sole pressure-induced phase transition predicted for $CsAgF_3$ salt is also associated with large changes of the first coordination sphere of Ag^{II}. The parent structure at 30 GPa features the following Ag–F bond lengths: 2×1.98, 2×1.99, and 2×2.11 Å. The post-perovskite structure **D** at 40 GPa shows two independent Ag sites, both with highly irregular Ag^{2+} coordination (one pentacoordinated: 1.97, 2.04, 2.10, 2.13, 2.34 Å, and another hexacoordinated: 1.99, 2.02, 2.13, 2.14, 2.23, 2.32 Å). Here, the former AgF_3^- chains polymerize into a complex 3D network. As in the case of K and Rb salts, the alkali metal cation experiences a counterintuitive decrease of the coordination number upon transition, with 12-coordinated Cs in the ambient-pressure tetragonal structure, and 11-coordinated Cs in the high-pressure structure.

The described structural transitions heavily impact magnetic properties of $MAgF_3$ perovskites. All ambient-pressure structures comprise linear or only slightly bent infinite AgF_3^- chains, which produce strong 1D antiferromagnetic superexchange.[10,11] The calculated J_{1D} values range from about −100 meV for the K salt, to −180 meV for the Cs analogue.[11] However, the **A**→**B** structural phase transition leads to bending of the Ag–F–Ag angle from 161° to 152° (for the K salt at the transition), and from 143° to 117° (for the Rb salt at the transition). An analogous **A**→**D** transition for Cs salt is also associated with remarkable reduction in the Ag–F–Ag angle from 180° to 159°. Not surprisingly, this implies that antiferromagnetic intra-chain superexchange energy must weaken substantially down to around −50 meV for K, and only −5 meV for Cs. Deformation of the Ag–F–Ag angle in the case of the Rb salt at 20 GPa is so pronounced (117°) that a weak ferromagnetic superexchange predominates (ca. +5 meV). In other words, increase of connectivity and structural dimensionality is associated with weakening of antiferromagnetic interactions.

Conclusions

Structural phase transitions for $MAgF_3$ perovskites (M=K, Rb, Cs) have been predicted theoretically for pressures up to 100 GPa; similarities were exhibited between $KAgF_3$ and $RbAgF_3$, from which $CsAgF_3$ differs starkly. Surprisingly, a decrease in the coordination number of the alkali metal is observed as pressure increases, and the critical pressure of the first transition rises together with the ionic radius of the alkali metal,[21] contrary to what is usually observed.[22] Release of the strain here is associated with compression of the Jahn–Teller-distorted $[AgF_6]^{4-}$ octahedron present in the low-pressure structures. This Jahn–Teller distortion of the $4d^9$ Ag^{2+} ions is key to the symmetry lowering in the high-pressure polymorphs of all the title compounds. While the second phase transition for K and Rb salts is associated with a formal increase in symmetry from monoclinic to orthorhombic, in structure **C**, in contrast to structure **A**, Ag does not sit at the special position, and its local coordination sphere is highly irregular.

The behavior of $KAgF_3$ contrasts strongly with that of $KCuF_3$,[23,24] which is actually isostructural with $CsAgF_3$, for which pressures as low as 8 GPa lead to significant reduction in the Jahn–Teller distortion without leading to any structural phase transition.[25] The very different behavior of Cu^{II} and Ag^{II} salts may be understood in terms of the much stronger covalence of the metal–fluorine bonds in the latter.[4,5] On the other hand, the behavior of $CsAgF_3$ seems to be unprecedented among fluoride perovskites. Although triclinic post-perovskites are known for $Ag^{I}Cu^{II}F_3$ and $Na^{I}Cu^{II}F_3$,[26] they lack the presence of a strongly polymerized MF_3^- anionic sublattice, such as the one seen in structure **D** of $CsAgF_3$.

For all members of the $MAgF_3$ series studied here, phase transitions impact the Ag–F–Ag angle that substantially decreases upon the phase transitions, and – in agreement with the Goodenough–Kanamori rules – this leads to substantial (from two- to 40-fold) weakening of the antiferromagnetic superexchange energy for K and Cs salts at the transition; in the case of Rb salt at 20 GPa, the Ag–F–Ag angle is already close to perpendicular, so weak ferromagnetism is predicted.

It is interesting to note that the $MAgF_3$ perovskites studied here display quite contrasting behavior to that of their cubic analogs (i.e., perovskites of the type KMF_3, where M = Mg, Zn, Co, Ni, and $CsMF_3$, where M = Ca, Cd, and the inverse perovskite $BaLiF_3$).[27–30] According to experiments and theoretical calculations, all these ideal perovskites retain cubic symmetry up to substantial pressures of 50–60 GPa, despite differences in Goldschmidt tolerance factors within this family of compounds.

Computational Details

Solid-state density functional theory (DFT) structural screening was carried out with using self-learning algorithms implemented in XtalOpt r11.0.[16,17] Aside from random structure generation, several structure types were manually fed into the structure pool. These were the available experimental structures and models prepared by $Ag^+ \rightarrow K^+$ substitutions of Ag_2F_3 and Ag_3F_4 high-pressure structures[31] (note that the ionic radii of Ag^+ and K^+ are quite similar). DFT calculations utilized the Perdew–Burke–Ernzerhof exchange-correlation functional,[32,33] and the projector-augmented-wave method[34] with appropriate pseudopotentials[35] from v.54 dataset as implemented in the VASP 5.4.4 code.[36] The cut-off energy of the plane wave basis set was equal to 950 eV with a self-consistent-field convergence criterion of 10^{-6} eV. The following number of formula units in the unit cell were tested: 2, 3, 4 and 6. Numerous equilibrium structures were obtained and symmetrized. In the second stage, the most promising (lowest enthalpy) structures obtained from preliminary screening were optimized in various ferromagnetic and antiferromagnetic models using the DFT $+U$ method with $U = 5.5$ eV and $J = 1.0$ eV.[37–39] Perdew–Burke–Ernzerhof exchange-correlation functional revised for solids (PBEsol)[40] functional was used with tight convergence criteria. For all structures their enthalpies were compared at each pressure to determine the minimum-enthalpy structures. In the final stage, to estimate the strength of magnetic superexchange, for each investigated external pressure one minimum-enthalpy structure was chosen and single-point energy calculations for different magnetic configurations were performed at the DFT $+U$ (PBEsol) level of theory.

All figures of structures were prepared by using VESTA.[41]

Acknowledgements

The research was supported by Polish National Science Center (NCN) and Deutsche Forschungsgemeinschaft (DFG) within BEETHOVEN2 project (2016/23/G/ST5/04320, KO 3990/8-1). Computations were carried out using resources of the Interdisciplinary Centre for Mathematical and Computational Modelling, University of Warsaw (grants G49-17 and GA83-34). Open Access funding enabled and organized by Projekt DEAL.

Conflict of Interest

The authors declare no conflict of interest.

Data Availability Statement

The data that support the findings of this study are available in the supplementary material of this article.

Keywords: fluorides · high pressure · magnetic superexchange · perovskites · phase transitions · silver

[1] T. M. Brenner, D. A. Egger, L. Kronik, G. Hodes, D. Cahen, *Nat. Rev. Mater.* **2016**, *1*, 15007.
[2] C. C. Stoumpos, C. D. Malliakas, M. G. Kanatzidis, *Inorg. Chem.* **2013**, *52*, 9019–9038.
[3] N. Bachar, K. Koteras, J. Gawraczyński, W. Trzcinski, J. Paszula, R. Piombo, P. Barone, Z. Mazej, G. Ghiringhelli, A. Nag, K.-J. Zhou, J. Lorenzana, D. van der Marel, W. Grochala, *Phys. Rev. Res.* **2022**, *in print*.
[4] W. Grochala, R. G. Egdell, P. P. Edwards, Z. Mazej, B. Zemva, *ChemPhysChem* **2003**, *4*, 997–1001.
[5] W. Grochala, R. Hoffmann, *Angew. Chem. Int. Ed.* **2001**, *40*, 2742–2781; *Angew. Chem.* **2001**, *113*, 2816–2859.
[6] J. Gawraczyński, D. Kurzydłowski, R. Ewings, S. Bandaru, W. Gadomski, Z. Mazej, G. Ruani, I. Bergenti, T. Jaroń, A. Ozarowski, S. Hill, P. J. Leszczyński, K. Tokár, M. Derzsi, P. Barone, K. Wohlfeld, J. Lorenzana, W. Grochala, *Proc. Natl. Acad. Sci. USA* **2019**, *116*, 1495–1500.
[7] T. Jaroń, W. Grochala, *Phys. Status Solidi RRL* **2008**, *2*, 71–73.
[8] D. Kurzydłowski, W. Grochala, *Angew. Chem. Int. Ed.* **2017**, *56*, 10114–10117; *Angew. Chem.* **2017**, *129*, 10248–10251.
[9] R. H. Odenthal, R. Hoppe, *Monatsh. Chem.* **1971**, *102*, 1340–1350.
[10] Z. Mazej, E. Goreshnik, Z. Jagličić, B. Gaweł, W. Łasocha, D. Grzybowska, T. Jaroń, D. Kurzydłowski, P. Malinowski, W. Koźminski, J. Szydłowska, P. Leszczyński, W. Grochala, *CrystEngComm* **2009**, *11*, 1702–1710.
[11] D. Kurzydłowski, Z. Mazej, Z. Jagličić, Y. Filinchuk, W. Grochala, *Chem. Commun.* **2013**, *49*, 6262–6264.
[12] K. Koteras, J. Gawraczyński, Z. Mazej, M. Derzsi, W. Grochala, *Chemistry* **2021**, *3*, 94–103.
[13] K. Koteras, J. Gawraczyński, G. Tavčar, Z. Mazej, W. Grochala, *CrystEngComm* **2022**, *24*, 1068–1077.
[14] A. Grzelak, J. Gawraczyński, T. Jaroń, D. Kurzydłowski, Z. Mazej, P. J. Leszczyński, V. B. Prakapenka, M. Derzsi, V. V. Struzhkin, W. Grochala, *Dalton Trans.* **2017**, *46*, 14742–14745.
[15] A. Grzelak, J. Gawraczyński, T. Jaroń, D. Kurzydłowski, A. Budzianowski, Z. Mazej, P. J. Leszczyński, V. B. Prakapenka, M. Derzsi, V. V. Struzhkin, W. Grochala, *Inorg. Chem.* **2017**, *56*, 14651–14661.
[16] D. C. Lonie, E. Zurek, *Comput. Phys. Commun.* **2011**, *182*, 372–387.
[17] P. Avery, C. Toher, S. Curtarolo, E. Zurek, *Comput. Phys. Commun.* **2019**, *237*, 274–275.
[18] W. Grochala, *Phys. Status Solidi B* **2006**, *243*, R81–R83.
[19] Z. Mazej, D. Kurzydłowski, W. Grochala, in *Photonic and Electronic Properties of Fluoride Materials* (Eds.: A. Tressaud, K. Poeppelmeier), Elsevier, Amsterdam, **2016**, p. 231.
[20] D. Kurzydłowski, M. Derzsi, A. Budzianowski, Z. Jagličić, W. Koźminski, Z. Mazej, W. Grochala, *Eur. J. Inorg. Chem.* **2010**, 2919–2925.
[21] M. Mantina, A. C. Chamberlin, R. Valero, C. J. Cramer, D. G. Truhlar, *J. Phys. Chem. A* **2009**, *113*, 5806–5812.
[22] W. Grochala, J. Feng, R. Hoffmann, N. W. Ashcroft, *Angew. Chem. Int. Ed.* **2007**, *46*, 3620–3642; *Angew. Chem.* **2007**, *119*, 3694–3717.
[23] M. W. Lufaso, P. M. Woodward, *Acta Crystallogr. Sect. B* **2004**, *60*, 10–20.
[24] N. Binggeli, M. Altarelli, *Phys. Rev. B* **2004**, *70*, 085117.
[25] J.-S. Zhou, J. A. Alonso, J. T. Han, M. T. Fernández-Díaz, J.-G. Cheng, J. B. Goodenough, *J. Fluorine Chem.* **2011**, *132*, 1117–1121.
[26] J. Tong, C. Lee, M.-H. Whangbo, R. K. Kremer, A. Simon, J. Köhler, *Solid State Sci.* **2010**, *12*, 680–684.
[27] G. Vaitheeswaran, V. Kanchana, R. S. Kumar, A. L. Cornelius, M. F. Nicol, A. Svane, A. Delin, B. Johansson, *Phys. Rev. B* **2007**, *76*, 014107.
[28] G. Vaitheeswaran, V. Kanchana, R. S. Kumar, A. L. Cornelius, M. F. Nicol, A. Svane, N. E. Christensen, O. Eriksson, *Phys. Rev. B* **2010**, *81*, 075105.

[29] G. Vaitheeswaran, V. Kanchana, X. Zhang, Y. Ma, A. Svane, N. E. Christensen, *J. Phys. Condens. Matter* **2016**, *28*, 315403.
[30] F. Aguado, F. Rodríguez, S. Hirai, J. N. Walsh, A. Lennie, S. A. T. Redfern, *High Pressure Res.* **2008**, *28*, 539–544.
[31] D. Kurzydłowski, M. Derzsi, E. Zurek, W. Grochala, *Chem. Eur. J.* **2021**, *27*, 5536–5545.
[32] J. P. Perdew, K. Burke, M. Ernzerhof, *Phys. Rev. Lett.* **1996**, *77*, 3865–3868.
[33] J. P. Perdew, K. Burke, M. Ernzerhof, *Phys. Rev. Lett.* **1997**, *78*, 1396.
[34] P. E. Blöchl, *Phys. Rev. B* **1994**, *50*, 17953–17979.
[35] G. Kresse, D. Joubert, *Phys. Rev. B* **1999**, *59*, 1758–1775.
[36] VASP version 5.4.4, Apr 2017.
[37] G. I. Csonka, J. P. Perdew, A. Ruzsinszky, P. H. T. Philipsen, S. Lebègue, J. Paier, O. A. Vydrov, J. G. Ángyán, *Phys. Rev. B* **2009**, *79*, 155107.
[38] D. Kasinathan, K. Koepernik, U. Nitzsche, H. Rosner, *Phys. Rev. Lett.* **2007**, *99*, 247210.
[39] J. Tong, J. Köhler, A. Simon, C. Lee, M.-H. Whangbo, *Z. Anorg. Allg. Chem.* **2012**, *638*, 1792–1795.
[40] J. P. Perdew, A. Ruzsinszky, G. I. Csonka, O. A. Vydrov, G. E. Scuseria, L. A. Constantin, X. Zhou, K. Burke, *Phys. Rev. Lett.* **2008**, *100*, 136406.
[41] K. Momma, F. Izumi, *J. Appl. Crystallogr.* **2008**, *41*, 653–658.

Manuscript received: March 7, 2022
Accepted manuscript online: March 29, 2022
Version of record online: May 3, 2022